Robust registration between cardiac MRI images and atlas for segmentation propagation

X. Zhuang[*a], D. J. Hawkes[a], W. R. Crum[a], R. Boubertakh[b], S. Uribe[b], D. Atkinson[a], P. Batchelor[b], T. Schaeffter[b], R. Razavi[b], D. L. G. Hill[a]
[a]Centre for Medical Image Computing, University College London, UK, WC1E 6BT;
[b]Interdisciplinary Medical Imaging Group, St Thomas' Hospital, KCL, UK, SE1 7EH

ABSTRACT

We propose a new framework to propagate the labels in a heart atlas to the cardiac MRI images for ventricle segmentations based on image registrations. The method employs the anatomical information from the atlas as priors to constrain the initialisation between the atlas and the MRI images using region based registrations. After the initialisation which minimises the possibility of local misalignments, a fluid registration is applied to fine-tune the labelling in the atlas to the detail in the MRI images. The heart shape from the atlas does not have to be representative of that of the segmented MRI images in terms of morphological variations of the heart in this framework. In the experiments, a cadaver heart atlas and a normal heart atlas were used to register to *in-vivo* data for ventricle segmentation propagations. The results have shown that the segmentations based on the proposed method are visually acceptable, accurate (surface distance against manual segmentations is 1.0 ± 1.0 mm in healthy volunteer data, and 1.6 ± 1.8 mm in patient data), and reproducible (0.7 ± 1.0 mm) for *in-vivo* cardiac MRI images. The experiments also show that the new initialisation method can correct the local misalignments and help to avoid producing unrealistic deformations in the nonrigid registrations with 21% quantitative improvement of the segmentation accuracy.

Keywords: Registration, Cardiac MRI, Segmentation, Label Propagation, Atlas

1. INTRODUCTION

In cardiac functional analysis, the quantitative computation of the functional descriptors from the cardiac MRI (CMRI) images is important, such as the myocardial wall thickening, wall motion, and ejection fraction, etc. Hence, accurate segmentations of the cardiac images are crucial in cardiac studies. Currently, most of the clinical applications use manual segmentations. However, the manual segmentation is not only tedious and time-consuming but also subjective to intra- and inter- observer error which results in inconsistent measurements. Recently, a number of publications have reported on automatic segmentation techniques by propagating a *priori* labels to the CMRI images. These techniques can be classified into two categories:

1. One is to build a statistical model from a group of training data and adapt the surface or boundary of the model to the corresponding boundaries in the segmented images based on the image intensity and/or gradient information [4, 5]. However, the construction of the statistical model [3] is also challenging because it needs a number of training data with already segmentations for each region; and the model has limited local adaptation flexibility which is determined by the input training data. Hence the training data used in the construction has to be representative of all possible heart shapes to achieve a high accuracy, which is practically more challenging than the segmentation itself.
2. The other is to use nonrigid registrations to register a pre-constructed heart atlas into the coordinate of these segmented images for label propagations. One example is to propagate a manual segmented MRI image on the end-diastolic phase to the other phases for the whole cardiac cycle segmentations based on nonrigid registrations. Another example is to construct an average atlas from the manual segmentations of a number of different subjects for the nonrigid registrations between the atlas and other subjects' data. These methods have been reported to be able to produce results with good correlations to the manual segmentations in [6-8] because

* x.zhuang@ucl.ac.uk; 44 207 679-0346

the nonrigid registration has a large number of degree of freedom (DOF) for local adaptations. However there is no anatomical constraint incorporated into the registrations in these methods; hence the atlas can be only used to register to the same subject or the subjects with similar heart shapes for the segmentation propagation. Therefore the atlas used has a limited impact on automating segmentation propagations across the population. The main reason for this limitation is that the initialisation method in these methods employs one single global transformation without a *priori* anatomical information and can produce local misalignments which can not be corrected by nonrigid registrations.

In this paper, we propose a new framework based on image registrations for the ventricle segmentation propagations in CMRI images. This framework uses a new initialisation method to incorporate the anatomical priors and the fluid registration with large DOF for fine-tuning the local adaptations.

- The initialisation method uses anatomical prominent regions in the atlas and constrains them to the corresponding regions in the CMRI images to minimise the possibility of the local misalignment. The "anatomical constraints" are introduced into the framework using region based registrations and can give a good starting estimate in terms of anatomical correspondence for the local adaptation in the nonrigid registration.
- The fluid registration which has a large number of DOF can flexibly adapt the morphologically initialised atlas into the detail of the CMRI images to achieve high segmentation accuracy.

In the following sections, we will firstly describe the initialisation using region based registrations (IRBReg) method and the registration framework for automatic ventricle segmentations in CMRI images in the methodology section. Then, in the experiment and result sections, three groups of experiments are employed to demonstrate the segmentation and evaluate the performance. The first two groups of experiments employ a cadaver heart atlas to register to the CMRI images: the first group uses four healthy volunteer and four patient data to visually demonstrate the robustness and accuracy; the second group employs five volunteer data which have two same-time scans to produce two anatomical identical images except artefacts and noises to assess the reproducibility of the segmentations. The third group applies an atlas built from a normal heart (healthy volunteer) to four patient and four healthy volunteer data for ventricle segmentations and assesses the accuracy against the manual segmentations. Conclusion and discussion are given in the last section.

2. METHOD

2.1 Initialisation using region based registrations

We propose a new initialisation method using region based registrations (IRBReg) to introduce the heart anatomical constraints into the initialisation stage for following nonrigid registrations. This method extracts some anatomically meaningful regions for one image, to register to the other image separately; and then combines all the resultant transformations into one displacement field using distance weighting interpolation to provide the starting estimate. For example, in cardiac atlas to MRI image registration, the morphological regions including ventricles, atriums, aorta, and artery can be extracted from the atlas into separate images to register to the MRI image to get the resultant transformations G_i and interpolate them into the starting estimate transformation T:

$$T(X) = \begin{cases} G_i(X), & X \in V_i,\ i = 1...n \\ f(X), & X \notin \bigcup_{i=1}^{n} V_i \end{cases} \quad (1)$$

where, V_i represents the regions which are related to the extracted regions of the atlas and have been guaranteed by the overlapping correction procedure (OCP) to be no overlapping between themselves after the corresponding resultant transformations. The OCP works by dilating the overlapped regions and then excluding the dilated regions from V_i. Assume that V_i' are all the extracted regions, such as chambers and arteries in the cardiac atlas image, and R_o' is the overlap region after the resultant transformations; then R_o is the region after a morphological dilation from R_o' using a d millimetre radius ball-shape structure element:

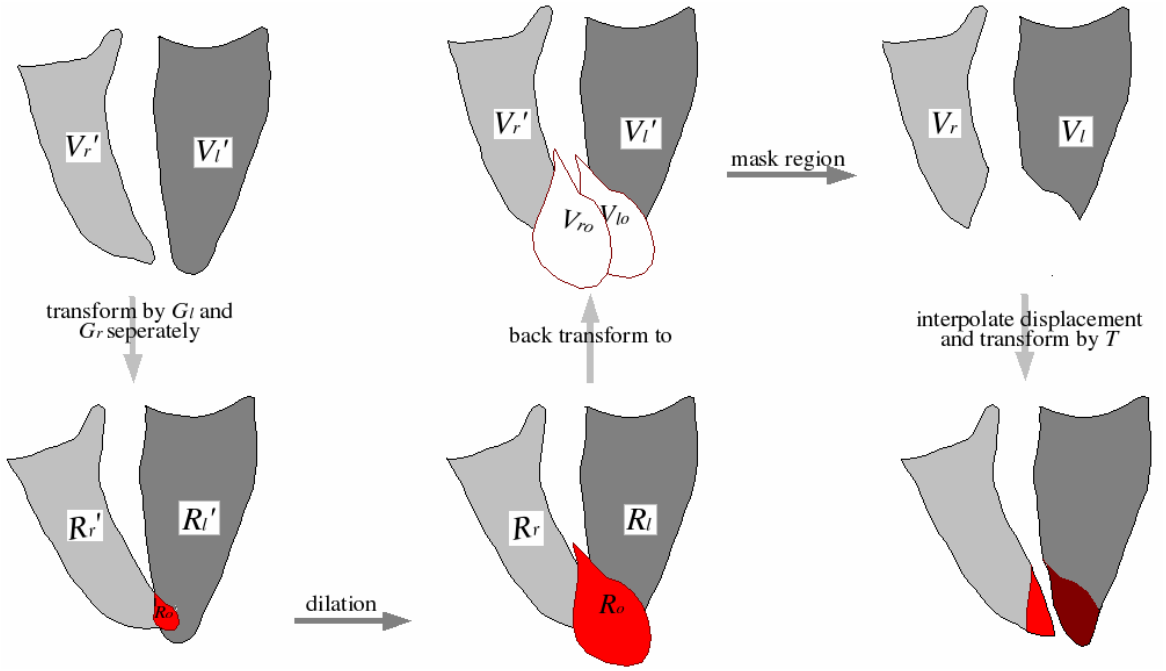

Fig. 1. A diagram demonstrating the overlapping correction procedure of the left and right ventricle cavities after two separate registrations. The dilation of the overlapped region is used to exclude the partial regions of the left and right ventricle cavities; The displacement of this region is interpolated based on the distance weighting interpolation.

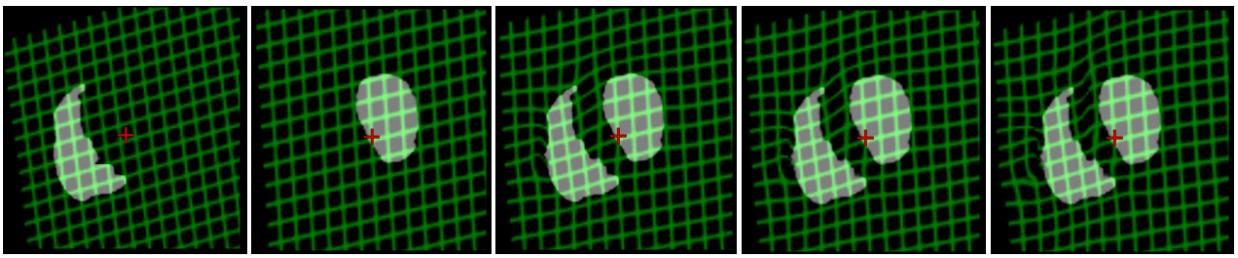

(a) (b) (c) (d) (e)

Fig. 2 The rigid transformation on the right ventricle cavity (a), the rigid transformation on the left ventricle cavity, and the transformation after interpolation based on the displacement of the two ventricle cavities choosing *e* value of 1.5 (c), 2 (d), and 4 (e).

$$R_o = \oplus_d \left\{ \bigcup \left[\bigcap_{i \neq j} \left(G_i(V_i'), G_j(V_j') \right) \right] \right\}, \tag{2}$$

and then the OCP corrected regions are:

$$V_i = V_i' - V_{io}, \qquad where, \;\; V_{io} = \left\{ x \mid x \in V_i' \cap G_i(x) \in R_o \right\}. \tag{3}$$

R_o ensures all V_i are overlap free before and after the corresponding affine transformations. Fig. 1 gives the flowchart of the computation of V_i for the left and right ventricle segmentations, where V_1 and V_2 for left and right ventricle cavities are denoted as V_l and V_r respectively and all the indexes of *1* and *2* are using *l* and *r* instead for denotation convenience. In our experiments, *d* is valued as 10 mm; however the choice of *d* value is not crucial in our experiments for two

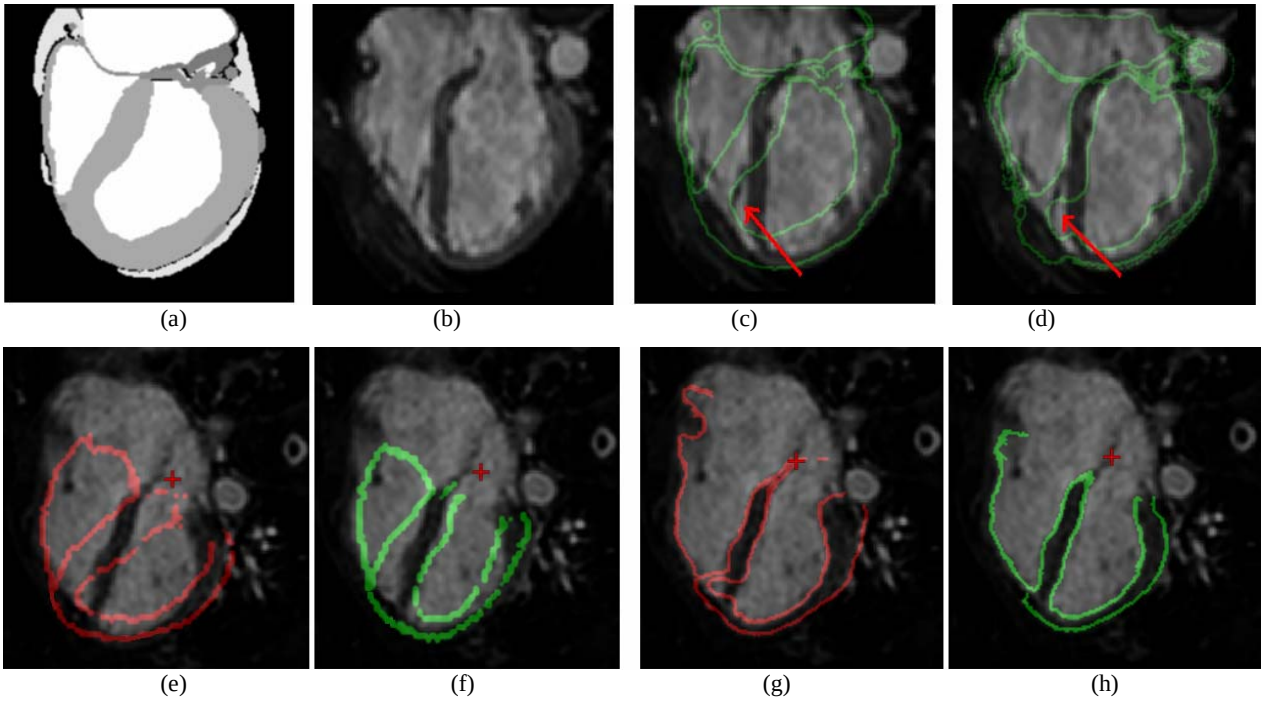

Fig. 3 The Images from different hearts: the atlas image from the voxel-man with some changes (a); and a volunteer data (b); the right ventricle blood pool of the MRI image overlaps with the left ventricle blood pool of the atlas after rigid registration – the arrow in (c); after nonrigid registration, the overlapped blood region is registered together and the myocardium is contracted to a minimum to make it least effectible for the intensity based similarity measure – the arrow in (d) shows a middle step of a nonrigid registration. (e)-(h) shows a segmentation on a pathologically dilated right ventricle patient data: (f) and (h) are the results after IRBReg and fluid registration; (e) and (g) are the results after affine and fluid registration without IRBReg.

reasons: (1) the overlap rarely happens in ventricle segmentations due to the septal myocardium between them; (2) in ventricle registrations, the affine registration in the IRBReg will scale the atlas ventricle blood pools down to exactly fit into the corresponding ventricle blood pools in the MRI image to avoid the left and right ventricle overlapping. However, the overlap correction can be crucial in other applications such as whole heart segmentation for atriums and arteries, where d value should be valued related to the original distance between the two regions and the biggest distance transformation value of the overlap regions.

After the overlapping correction, the distance weighting interpolation [1, 2] is employed to interpolate the transformation between V_i:

$$f(X) = \sum_{i=1}^{m} w_i(X) \times G_i(X_i), \tag{4}$$

where, $w_i(X)$ is the distance weighting function for X, and X_i is the nearest point to X in V_i.

$$w_i(X) = \frac{1/d_i(X)^e}{\sum_{i=1}^{m} 1/d_i(X)^e}. \tag{5}$$

where $d_i(X)$ is the Euclidean distance between point X and the region V_i. The smoothness of the displacements after the interpolation is determined by the choice of e (e>1 guarantees the first derivative is continuous) and the larger of e valued the more weighting the short distance points will have in the interpolation. Fig. 2 gives the deformation fields of interpolation results by e value of 1.5, 2, and 4 for the two ventricle segmentation applications. Based on the

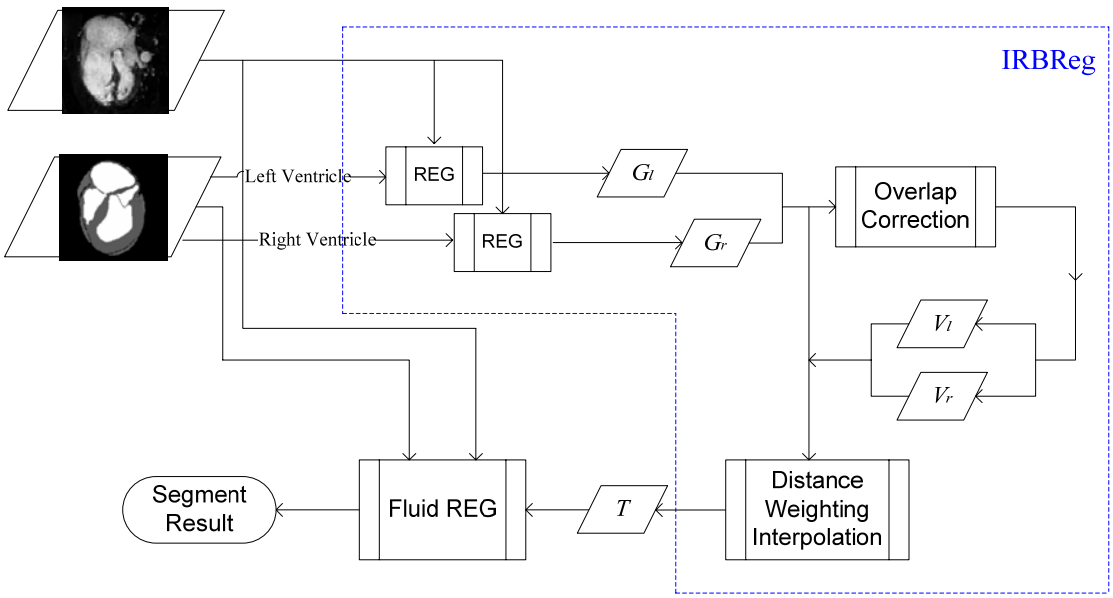

Fig. 4 The cardiac ventricle segmentation framework by means of propagating the labelling in a heart atlas to the detail of CMRI images based on IRBReg (in blue dash region) and fluid registration.

consideration of both smoothness and computation efficiency, a value of 2 whose result doesn't have significant difference to that of 1.5 which was proposed in [2] is used in the experiments next section.

In fig. 4, the blue coloured dash region demonstrates the IRBReg idea in the ventricle registration example.

2.2 Automatic ventricle segmentation using atlas-CMRI registrations

One should note that there are two challenges in the automatic segmentation of the CMRI images using inter-subject registration techniques.

First is to achieve a good starting estimate to initialise the anatomical correspondence between the atlas and the MRI image. This is essential to achieve a successful inter-subject nonrigid registration when their shapes have big variations, such as heart images. A good initialisation can help minimising the possibility of local misalignments. Fig. 3 (a)-(d) shows an example when a global affine transformation between a heart atlas (a) and a CMRI image (b) gives a starting estimate which has anatomical correspondence error in the apical region of the ventricles: the left ventricle of the atlas overlaps the right ventricle of the MRI image (c); finally, the nonrigid registration fails to correct the overlapped region (d). Therefore, the IRBReg method described above is employed to initialise the correspondence between the atlas and the MRI image based on the anatomical information of the heart.

The second challenge is the nonrigid registration between the atlas and the MRI images. Since the atlas we propose to use does not have to be built from special modality images, the atlas is not expected to have the same intensity information as the MRI images. Therefore, a multi-modality registration similarity measure is needed in this registration task – one should notice the normalized mutual information (NMI) method which is widely used for multi-modality image registrations [11]. Furthermore, the transformation model used in the nonrigid registration needs a large number of DOF to achieve the high accuracy which determines the performance of the segmentation. In this paper, the fluid deformation model is used in [9, 10] in the nonrigid registration because the diffeomorphism of the fluid deformation model is guaranteed by the physical mechanics which is practically easier to control than by introducing a smoothness constraint term into the cost function with a weighting factor.

Based on the IRBReg and fluid registration, we propose a framework for automatic ventricle segmentations from CMRI images which many cardiologists are interested in for clinical diagnosis and researches. Firstly, a heart atlas which has every anatomically prominent region labelled, such as left, right ventricle blood pools, and myocardium, is employed in

the framework. These labelled regions can be extracted from the atlas into independent images as a *priori* knowledge to separately register to the CMRI image in the IRBReg. Then, the fluid registration [9, 10] is used to fine-tune the labelling in the atlas to the detail in the MRI image while also minimizing the possibility of producing anatomically unrealistic deformations between the atlas and the MRI image. Since the atlas has labelled all the regions, a mask image which has all blood pool can be easily extracted from the atlas and applied to the fluid registration to practically improve the registration' robustness and decrease the run-time. This is because in inter-subject cardiac image registrations, the blood pool region normally needs much larger deformation fields than the myocardium. Hence, before applying the full heart fluid registration, the blood-pool-mask based fluid registration is firstly applied to correct most of the difference between them. Furthermore, to maximize the information of the images used in the NMI computation, we propose to compute the joint intensity probabilities p_{ms}, entropies H_A, H_B, and H_{AB} (please refer to [9] for detail) based on the whole images while compute the force (gradient of the similarity) on the mask regions for solving the partial differential equation (PDE) in the fluid registration:

$$Force(X) = \begin{cases} Gradient(X), & X \in V_{blood} \\ 0, & X \notin V_{blood} \end{cases} \tag{6}$$

This can save 80~90% run-time for computing the fluid force.

Fig. 4 gives the flowchart of the proposed framework for cardiac ventricle segmentations.

3. EXPERIMENTS

Three groups of experiments are employed to demonstrate the performance of the proposed segmentation framework based on the IRBReg and the fluid registration on cardiac MRI images. The cadaver atlas used in the first two groups was from http://www.voxel-man.de, as shown in fig. 3 (a) with a few changes. The voxel size of this atlas is 0.6mm*0.6mm*0.6mm. The other atlas used in the third group of experiments was built from a healthy volunteer with voxel size 0.5mm*0.5mm*0.5mm.The MRI sequence is the balanced steady state free precession (b-SSFP) for whole heart imaging from a 1.5T clinical scanner (Philips Medical System, Best, The Netherlands) equipped with 32 independent receive channels. The free breathing scan is realized by enabling one navigator beam before data acquisition and the trigger delays of the end-diastolic phase is selected manually with a preview T2 preparation and FAT saturation pulse. The gating window for the free breathing is controlled to be around 6mm in volunteers' acquisition given the volunteers have received a breath-with-regular-pattern training; while this is not guaranteed for the patient data acquisitions.

In the first group of experiments, we employ four health volunteers and four patients with abnormal heart shape due to dilated right ventricle or after valve replacement surgeries to visually assess the accuracy of the segmentations. The volunteer MRI data were scanned with acquisition resolution around 1.7mm*1.7mm*1.7mm and same reconstructed resolution based on short-axis view, and the patient MRI data were scanned with acquisition resolution 2mm*2mm*2mm and reconstructed to 1mm*1mm*1mm based on sagittal view.

In the second group of experiments, images from interleaving scans which acquire two k-space data at the same time from a subject to construct two images that have exact the same anatomy information but different noise and artefacts, and images from test-re-test scans which acquire two images successively are used to assess the reproducibility of the segmentation results. Three evaluation factors are computed for the assessment: volume size difference, volume overlap $((A \cap B)/(A \cup B))$ [12], and the endocardial and epicardial surface distance between the two results. Five subjects are included in this experiment and one were scanned based on short-axis view with acquisition resolution 1.7mm*1.7mm*1.7mm and same reconstructed resolution, others were based on sagittal view with both acquired and reconstruction resolution 1.6mm*1.6mm*1.6mm.

Finally, we use an atlas built from a normal heart for the segmentation propagation to segment another four health volunteer data with acquisition resolution 2mm*2mm*2mm and reconstructed to 1mm*1mm*1mm based on sagittal view and the four patient data used in the first group of experiment. The manual segmentation results on these data are employed to quantitatively evaluate the accuracy of the segmentations from both the proposed method and the method without the IRBReg.

Table 1 Segmentation results against manual segmentations. Here gives the error percentage distribution. Endo-LV means the endocardial surface of left ventricle, Endo-RV is the endocardial surface of right ventricle, and Epi-LV denotes the epicardial surface around left ventricle.

		0-1mm	1-2mm	2-3mm	3-4mm	4-5mm	>5mm
Volunteer Data	Endo-LV	78%	16%	3%	1%	0.6%	1%
	Endo-RV	69%	23%	5%	1%	0.8%	0.6%
	Epi-LV	62%	18%	9.5%	5.1%	2.6%	2.0%
Patient Data	Endo-LV	45%	22%	15%	7%	3%	7%
	Endo-RV	40%	20%	14%	9%	6%	11%
	Epi-LV	46%	24%	15%	7%	4%	4%

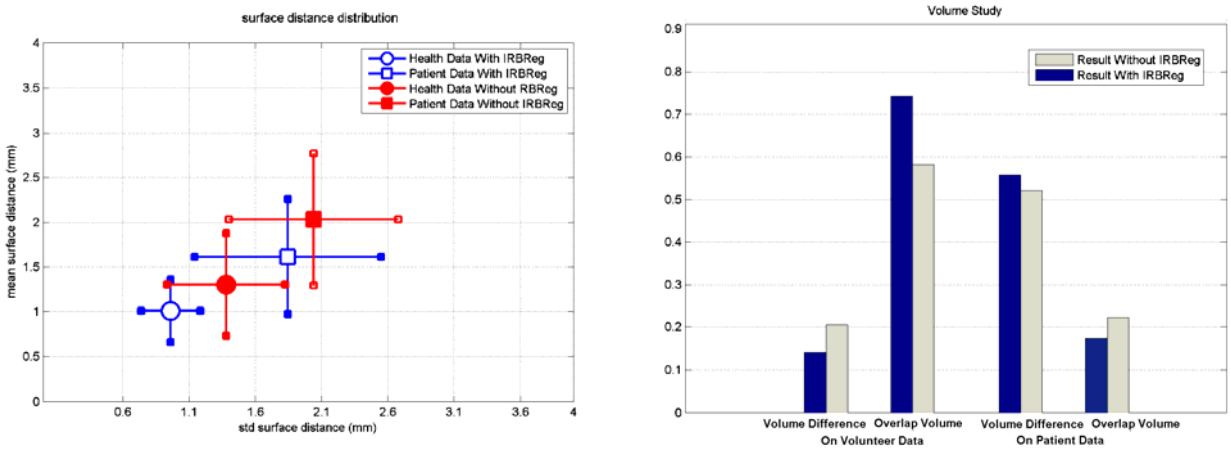

Fig. 5 The mean surface distance distribution and standard deviation of the surface distance from volunteer data and patient data (left); and the average overlap volume factor and volume difference of them (right). This figure shows the difference between the segmentation results by using the IRBReg method for initialisation and without IRBReg.

4. RESULTS

In our experiments, all ventricle segmentations are visually successful. Fig. 6 and fig. 7 give the three orthogonal views of the four patient and four health volunteer segmentation results on the cardiac ventricles in the first group of experiments. The visual observation from the segmentation results show that: (1) the segmentation is better at the endocardial surface where the boundary is clear than at the epicardial surface where some boundary is indistinct; however the segmentation of the papillary muscle is hard to control whether to be included or excluded from the myocardium; (2) the accuracy of the surface segmentation on the right ventricle is not always worse than that on the left ventricle though the tricuspid and pulmonary valves are more variable than mitral and aortic valves in label propagations especially in the pathological data with dilated right ventricles; (3) the segmentation at the regions which have adjacent tissues, the segmentation is less accurate but still acceptable because the force-masking fluid registration take the whole image information and is able to keep the heart shape from the prior shape information of the atlas; (4) the segmentation is robust from most of the MRI artefacts; (5) the valve boundaries segmentation which fails most of the other automatic segmentation methods which are based on image intensity gradient also addresses a difficult tasks for the proposed method because there is not obvious difference between the valves and the blood in the MRI images, but we still get

acceptable accuracy from the propagation; (6) finally, the segmentations on healthy volunteer are better than on pathological data in terms of accuracy. This is because the gating window for free-breathing navigating is normally set to wider in the MRI acquisition for the patients due to the uncontrollable breathing patterns of the patients. The wider gating window results in heavier motion artefacts from the breathing motions. The image quality can be visually evaluated with big difference between healthy and patent data from fig. 6 and fig. 7.

The average volume difference for the segmented left, right ventricle cavities, and the myocardium in the reproducibility experiment are 1.2%, 7.8%, and 5.1% respectively; and the overlap are 0.87, 0.76, and 0.75 respectively. The average surface distance, including the endocardial surface and epicardial surface of the ventricles, is 0.7 ± 1.0 mm. The method has shown good reproducibility of the ventricle segmentations from the surface distance although the volume difference and overlap volume factor are largely dominated by the valve definition variations. The relatively low reproducibility of the valves definition suggests that a re-definition of the valve position by covering the chambers with a flat plane after the segmentation should give a more reproducible chamber separation than label propagation from the atlas. This will be one of our future works.

After using the cadaver atlas for segmentation propagations in the first two groups of experiments, we use another atlas from a healthy heart volunteer's in the third group of experiments. Table 1 gives the error distribution for the endocardial surface of the left and right ventricles, and the epicardial surface of the left ventricles: overall around 90% of the regions are less than 2mm on the volunteer data and 66% on the patient data. Fig. 5 (a) gives the mean surface distance and standard deviation distribution from the four healthy volunteer and four patient data using the segmentation method proposed in this paper and the method without the IRBReg method. The mean surface distance by the proposed method on the four volunteers is overall 1.0 ± 0.2 mm for mean surface distance and 1.0 ± 0.4mm for standard deviation, and 1.8 ± 0.7mm and 1.6 ± 0.6mm respectively on the four patient data; while without the IRBReg method the surface distance is mean 1.3 ± 0.6mm and standard deviation 1.4 ± 0.5mm on the volunteer data, and mean 2.0 ± 0.8mm and standard deviation 2.0 ± 0.7mm on the patient data. Fig. 5 (b) give the average volume overlap and volume difference of the segmentation results. The results from this group of experiments show that the accuracy on the patient data is worse than on volunteer data, which confirms the visual evaluation conclusions in the first group of experiments. Fig 5 also shows that there is no drastic improvement from the IRBReg in terms of the quantitative evaluation. This is because the flexibility of the fluid registration is able to register the boundary between the atlas and MRI images thank to the thickness of the septal myocardium. Fig .3 (e) – (h) show a pathological heart disease data case segmented by the methods with and without the IRBReg. One can notice the visually significant difference between the two segmentation results. In this paper, we do not given the evaluation on the right ventricle epicardial surface because the thickness of the right ventricle myocardium on the end-diastolic phase is comparable to the segmentation error and the epicardial surface on right ventricle is hard to manually delineate due to the limitation of the visualisation in our segmentation tool.

The average runtime for one dataset segmentation with selected region of interest (heart region) is about 20-30 minutes on a 2.66GHz 16G RAM computer.

5. CONCLUSIONS

In this paper, we propose a segmentation framework for cardiac MRI images based on two steps: (1) a new initialisation method using the region based registrations (IRBReg) and (2) the fluid registration which has large number of DOF to align the local details. The IRBReg method introduces the anatomical constraints into the initialisation stage to minimise the possibility of local misalignment in the inter-subject registrations, which makes the atlas independent from the segmented data in terms of the heart shape variations. The flexible deformation model of the fluid registration can accurately fine-tune the label propagation from the atlas to the detail in the MRI images. In the experiments, the results have shown that the ventricle segmentations are visually acceptable (from fig. 6 and fig. 7), accurate (1.0 ± 1.0 mm on healthy volunteer data and 1.8 ± 1.6mm on patient data), and reproducible (0.7 ± 1.0 mm) for *in-vivo* CMRI datasets. Fig. 3 shows the advantages of the new initialisation method for local correction and the final segmentation accuracy, which compares with the results without the IRBReg. The average performance by the proposed segmentation method is 1.4 ± 1.3mm; while without the IRBReg, the segmentation accuracy is 1.7 ± 1.7mm. Finally, the proposed segmentation framework is not restricted in ventricle segmentations. It is potentially able to be applied to the whole heart segmentation which is more challenging. The IRBReg method can also be applied to other applications where the nonrigid registrations fail due to local misalignments in the initialisation derived from a single affine transformation. In our future

work, we will apply the segmentation method on the whole heart segmentations, to different modality heart images, and evaluate the results on more different pathological patient data.

ACKNOWLEGEMENT

This work was funded by EPSRC grant GR/T11395/01. The authors would like to thank Dr. Sebastien Ourselin for reviewing the paper prior to the submission and providing valuable feedback and Dr. Kawal Rhode for the helps on the manual segmentations and building the atlas.

REFERENCES

[1] D. Shepard, "A two-dimensional interpolation function for irregularly-spaced data," in Proc, 23rd national Conference of the ACM, ACM Press, 517-527 (1968).

[2] J. A. Little, D. L. G. Hill, D. J. Hawkes, "Deformation incorporating rigid structures," Computer Vision and Image Understanding, **66(2)**, 223-232 (1997).

[3] T. F. Cootes, C. Beeston, G. J. Edwards, C.J. Taylor, "A Unified framework for atlas matching using active appearance models," IPMI'99, LNCS 1613, 322-333 (1999).

[4] S. C. Mitchell, J. G. Bosch, B. P. F. Lelieveldt, R. J. van der Geest, J. H. C. Reiber, M. Sonka, "3-D active appearance models: segmentation of cardiac MR and ultrasound images," TMI, **21(9)**, 1167-1178 (2002).

[5] A. F. Frangi, D. Rueckert, J. A. Schnabel, W. J. Niessen, "Automatic construction of multiple-object three-dimension statistical shape models: application to cardiac modeling," TMI, **21(9)**, 1151-1166 (2002).

[6] M. Lorenzo-Valdes, G. I. Sanchez-Ortiz, R. Mohiaddin, D. Rueckert, "Atlas-based segmentation and tracking of 3D cardiac MR images using non-rigid registration," in Proc. MICCAI 2004, 189-192 (2002).

[7] R. M. Lapp, M. Lorenzo-Valdes, D. Rueckert, "3D/4D cardiac segmentation using active appearance models, non-rigid registration and the Insight Toolkit," in Proc. MICCAI 2004, 419-426 (2004).

[8] D. Perperidis, R. Mohiaddin, D. Rueckert, "Construction of a 4D statistical atlas of the cardiac anatomy and its use in classification," in Proc. MICCAI 2005, 402–410 (2005).

[9] W. R. Crum, D. L.G. Hill, D. J. Hawkes, "Information theoretic similarity measures in non-rigid registration," in Proc. IPMI 2003, LNCS 2732, 378–387 (2003).

[10] W. R. Crum, C. Tanner, D. J. Hawkes, "Anisotropic multi-scale fluid registration: evaluation in magnetic resonance breast imaging," Phys. Med. Biol. 50(031-9155 (Print), 21), 5153-5174. ISSN: 0031-9155, 2005

[11] C. Studholme, D.L.G. Hill, D.J. Hawkes, "An overlap invariant entropy measure of 3D medical image alignment," Pattern Recognition 32, 71-86 (1999).

[12] W. R. Crum, O. Camara, D. L. G. Hill, "Generalized overlap measures for evaluation and validation in medical image analysis," TMI, **25(11)**, 1451-1461 (2006).

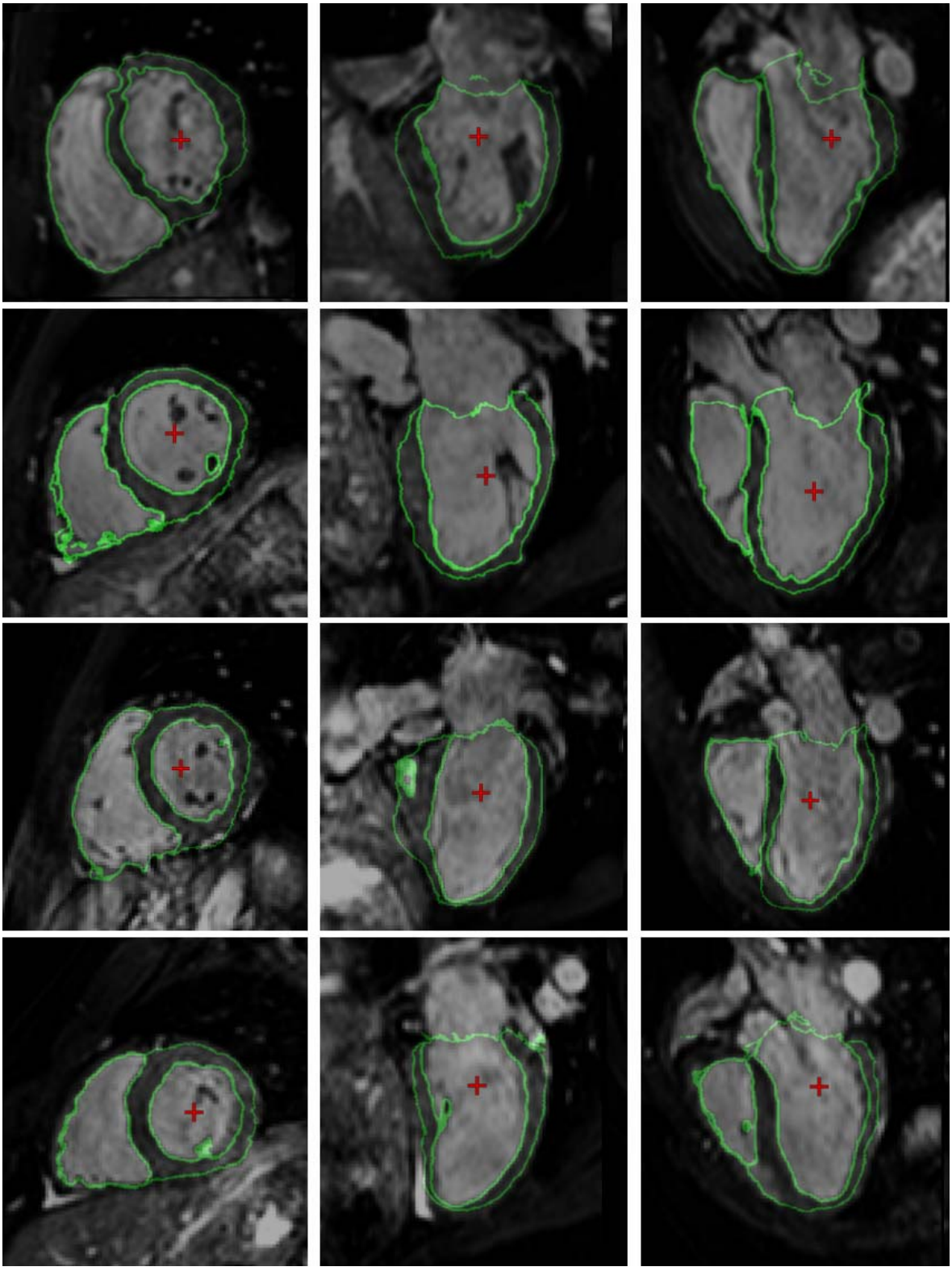

Fig. 6 The ventricle segmentation results on health volunteers' data.

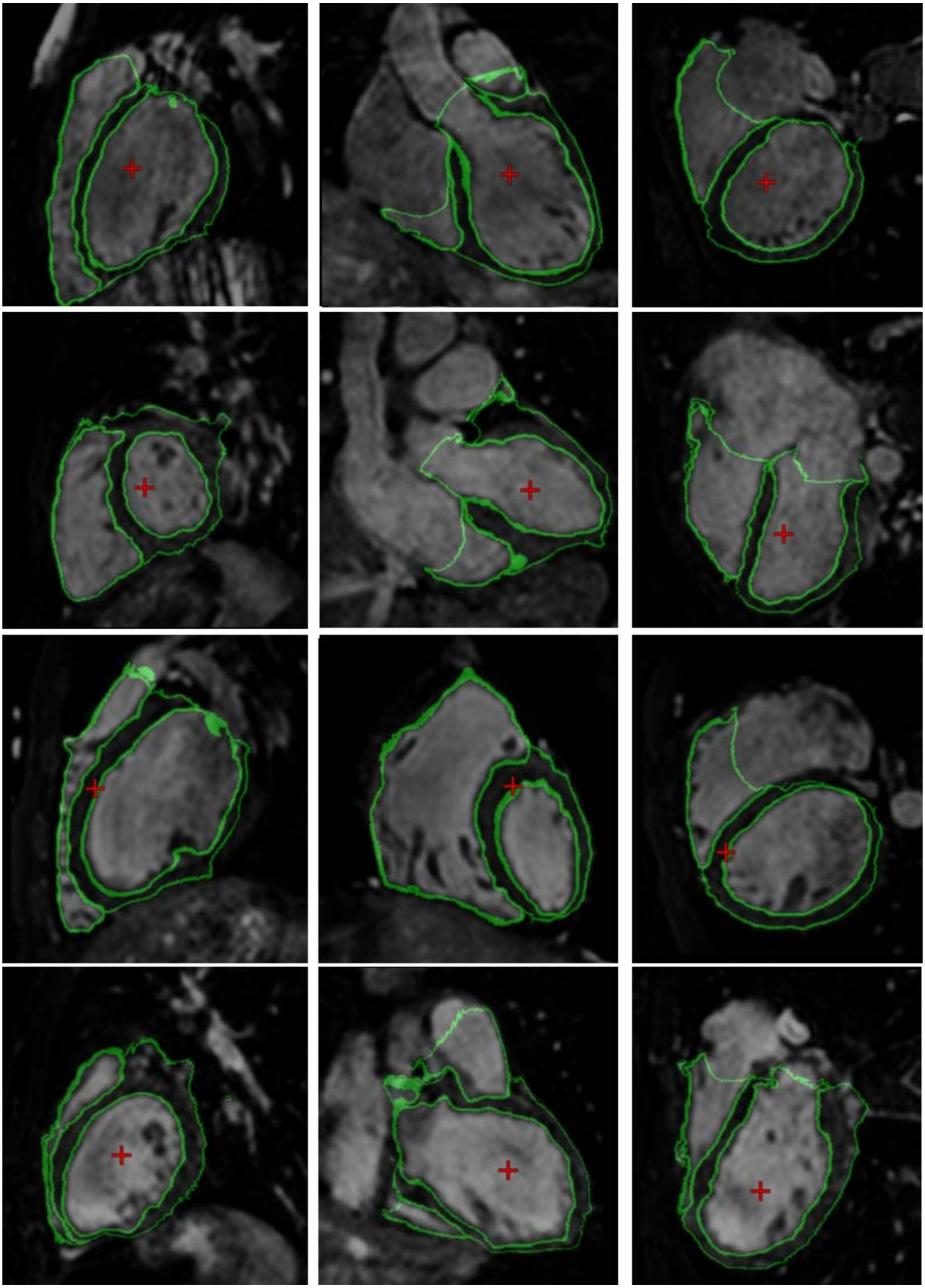

Fig. 7 The ventricle segmentation results on patients' data.